

Selection Rules for Resonant Inelastic X-Ray Scattering from Tetragonal Copper-Oxides

P. Abbamonte^{1,2,*}, C. A. Burns³, E. D. Isaacs², P. M. Platzman², L. L. Miller⁴, and M. V. Klein¹

¹*Department of Physics, University of Illinois, 1110 W. Green St., Urbana, IL, 61801*

²*Bell Laboratories, Lucent Technologies, 600 Mountain Av., Murray Hill, NJ, 07974*

³*Department of Physics, Western Michigan University, Kalamazoo, MI, 49008*

⁴*Ames Laboratory, Ames, IA, 50011*

(April 26, 2024)

We demonstrate the utility of point group representation theory for symmetry analysis in resonant inelastic x-ray scattering. From its polarization-dependence, we show that a 5 eV inelastic feature in $\text{Sr}_2\text{CuO}_2\text{Cl}_2$ has pure B_{1g} symmetry and assign it to a transition in the cell-perturbation calculations of Simon *et. al.* [Phys. Rev. B., **54**, R3780 (1996)]. We discuss how Raman selection rules are broken at nonzero momentum transfer and how this can also act as a probe of wave function symmetry.

PACS numbers: 78.70.Ck, 71.20.-b, 74.25.Jb

The two advantages of resonant as compared to nonresonant inelastic x-ray scattering are that it can be applied to high-density materials (where nonresonant techniques have problems with absorption) and its sensitivity to wave function *symmetry*. The former is well-documented but the latter has only recently been applied to solids by Duda [7] and Kuiper [8].

In this article we demonstrate the utility of point group representation theory for symmetry analysis in resonant inelastic x-ray scattering (RIXS). We focus on inelastic features which are brought about by the coulomb interaction between core and valence electrons. In different contexts such features have been called “forbidden excitonic” transitions [1], “indirect” transitions [2], “Coster-Kronig” features [3], “Auger resonant Raman” features [4], and “shakeup” features [5,6]. One expects these transitions to dominate K-edge RIXS spectra from d -electron systems with inversion symmetry (i.e. many transition metal oxides) owing to the absence of dipole-allowed transitions at the Brillouin zone center. We take the “shakeup” approach of Refs. [5,6] and tabulate the Raman-active symmetries in all independent experimental geometries. Comparing our polarization-dependent measurements of the 5 eV inelastic feature in $\text{Sr}_2\text{CuO}_2\text{Cl}_2$ (SCOC) (observed also in Nd_2CuO_4 [10] and La_2CuO_4 [6]) with the cell-perturbation calculations of Simon [9] we identify this feature to be a localized transition of B_{1g} (or $d_{x^2-y^2}$) symmetry. We conclude by discussing how selection rules are broken at nonzero momentum transfer and how this can act as an additional probe of wave function symmetry.

Experiments were carried out at the 3ID (SRI-CAT) beam line at the Advanced Photon Source using a 6-circle diffractometer with an analyzer stage. Energy analysis of the scattered light was done with a spherical Ge(733) analyzer working near backscattering. The overall energy resolution was 0.9 eV, and with 6×10^{12} phonons/sec on the sample typical inelastic count rates were 10 Hz. The

scattering angle in the experiment was fixed at $2\theta = 16^\circ$, allowing detection of both parallel and crossed polarization. Two detectors were employed so fluorescence yield data could be taken simultaneously with RIXS measurements.

The crystals were grown as described previously [11], cut to (100) and (001) surfaces, and polished with a $1 \mu\text{m}$ AlO film. This allowed variation of the incident polarization, $\hat{\epsilon}_i$, and the momentum transfer, \mathbf{q} , independently with respect to the crystal axes. The surface quality was verified with Laué photos and an FTIR reflectometer.

Figure 1 shows spectra taken with $\hat{\epsilon}_i \parallel \hat{\mathbf{x}}$ and $\mathbf{q} = (1.27 \text{ \AA}^{-1})\hat{\mathbf{z}}$. The incident energy, ω_i , was varied from 8988 eV to 9006 eV to generate a resonance profile. A feature at 5 eV energy loss is visible and resonates in a complex fashion. It sits on a flat, incoherent, multi-electron/phonon continuum which does not change with ω_i . This continuum is analogous to the selection rule-violating features seen in RIXS from molecules [12,13,14] which occur because of interference of vibrational modes. It could in principle be disposed of by detuning [12,13,14], however it is featureless and so presents no problem for data interpretation [15].

The coherent feature at 5 eV energy loss has been shown to be an “indirect” transition [10,6], and is what we wish to symmetry-analyze. We use the “shakeup” approach of Refs. [5,6] to describe the coupling of x-rays to this excitation. This approach uses the weakness of the coulomb interaction (the expansion parameter being $\alpha=1/137$) to describe the resonance process analytically in perturbation theory, and works as long as the coulomb interaction brings about no topological change in the $4p$ band states (this is the case if the $4p$ bandwidth is large, as it is in this case). We neglect here the detailed energy structure of intermediate states since we plan to make only general symmetry arguments.

According to Ref. [6] the spectra in Figure 1 can be described by the expression

$$w_{i \rightarrow f} = \frac{S_K(\mathbf{q}, \omega; \hat{\epsilon}_i, \hat{\epsilon}_s)}{[(\omega_i - E_K)^2 + \gamma_K^2][(\omega_s - E_K)^2 + \gamma_K^2]}, \quad (1)$$

where the function S_K is independent of ω_i and the spectral changes in Figure 1 are accounted for entirely by the energy denominators [the doublet structure in the open circles comes from the double denominator [16]]. S_K contains information about Raman selection rules and has the form [6]

$$S_K(\mathbf{q}, \omega; \hat{\epsilon}_i, \hat{\epsilon}_s) = \frac{2\pi}{\hbar} \sum_f \left| \sum_{\bar{1}s4p} M_{em} M_{coul} M_{abs} \right|^2. \quad (2)$$

To derive selection rules we discuss the role each of these three matrix elements plays in the scattering process. For simplicity we begin in the optical limit ($\mathbf{q}=0$) and later discuss how selection rules are broken as \mathbf{q} is increased.

The action of M_{abs} is to annihilate the incident photon and create a virtual $\bar{1}s4p$ pair. In the dipole approximation the symmetry axis of the $4p$ is parallel to the incident polarization, $\hat{\epsilon}_i$ (provided $\hat{\epsilon}_i$ is along a principal axis). M_{em} annihilates the $\bar{1}s4p$ state and creates the scattered photon with polarization $\hat{\epsilon}_s$ again parallel to the $4p$.

The relationship between $\hat{\epsilon}_i$ and $\hat{\epsilon}_s$ depends on the action of M_{coul} , which determines how the $\text{Cu}\bar{1}s4p$ state couples to the valence electron system. M_{coul} has the explicit form

$$M_{coul} = -e^2 \int d\mathbf{x} d\mathbf{x}' \frac{\psi_{\bar{1}s'}^*(\mathbf{x}') \psi_{\bar{1}s}(\mathbf{x}') \psi_f^*(\mathbf{x}) \psi_i(\mathbf{x})}{|\mathbf{x} - \mathbf{x}'|} \quad (3)$$

$$+ e^2 \int d\mathbf{x} d\mathbf{x}' \frac{\psi_{4p'}^*(\mathbf{x}') \psi_{4p}(\mathbf{x}') \psi_f^*(\mathbf{x}) \psi_i(\mathbf{x})}{|\mathbf{x} - \mathbf{x}'|} \quad (4)$$

plus exchange terms. These integrals describe the coulomb interaction between core and valence electrons and have the familiar form of nonrelativistic electron-electron scattering in the Born approximation. Raman selection rules are determined by whether these integrals vanish (or not) by symmetry.

It is straight-forward to show [16] that the point group symmetries contained in the integrands (3-4) are given by the Krönecker product

$$\Gamma(\psi_{4p'}^* \psi_{4p} - \psi_{\bar{1}s'}^* \psi_{\bar{1}s}) \otimes \Gamma(\psi_f^* \psi_i), \quad (5)$$

where $\Gamma(f)$ represents the symmetry of the function f . According to the fundamental matrix element selection rule theorem [17] M_{coul} vanishes unless this quantity contains the identical representation, A_{1g} . Or equivalently, M_{coul} is nonzero if and only if the quantities $\Gamma(\psi_f^* \psi_i)$ (the overall symmetry of the valence excitation) and $\Gamma(\psi_{4p'}^* \psi_{4p} - \psi_{\bar{1}s'}^* \psi_{\bar{1}s})$ (determined entirely by the experimental geometry) share at least one common symmetry. In other words - *and this is the key point* - the Raman active symmetries for a given experimental

geometry are the symmetries contained in the quantity $\Gamma(\psi_{4p'}^* \psi_{4p} - \psi_{\bar{1}s'}^* \psi_{\bar{1}s})$, which depends only on the experimental geometry.

In the optical limit ($\mathbf{q}=0$) $\Gamma(\psi_{1s}) = a_{1g}$, since a $\text{Cu}1s$ orbital is invariant under all point group operations (Cu sits at an inversion center in SCOC). So the quantity (5) reduces to $\Gamma(\psi_{4p'}^*) \otimes \Gamma(\psi_{4p}) + A_{1g}$. We conclude that transitions of A_{1g} symmetry will be Raman-active in all experimental geometries. Furthermore, differences in selection rules between different experimental geometries are entirely determined by the $4p$.

We now derive the complete selection rules for one experimental geometry and then state the results for the others. Consider the case $\hat{\epsilon}_i || \hat{\mathbf{x}}$ and $\hat{\epsilon}_s || \hat{\mathbf{y}}$. In this case the $4p$ is initially oriented along $\hat{\mathbf{x}}$, but by action of M_{coul} it gets rotated along $\hat{\mathbf{y}}$. The symmetries contained in M_{coul} in this case are $\Gamma(4p_y) \otimes \Gamma(4p_x) + A_{1g}$. $4p_x$ and $4p_y$ have purely e_{ux} and e_{uy} symmetry, respectively, and $e_{ux} \otimes e_{uy} = B_{2g}$. So the Raman active symmetries in this geometry are $A_{1g} + B_{2g}$. Using this procedure one can generate Raman selection rules for all independent experimental geometries. The results are shown in Table 1.

Returning to the issue of the symmetry of the 5 eV inelastic feature, in Fig. 1 the incident polarization was $\hat{\mathbf{x}}$ and the scattered light was unpolarized, so the symmetry reflected in Fig. 1 is $A_{1g} + B_{1g} + B_{2g} + E_{gx}$ (see Table 1).

In Figure 2 we show spectra again with $\hat{\epsilon}_i || \hat{\mathbf{x}}$, but with \mathbf{q} now parallel to $\hat{\mathbf{y}}$. In the $\mathbf{q}=0$ limit this geometry contains the same Raman-active symmetries as Figure 1, and in fact the spectra are not observably changed. We therefore tentatively assume that we can apply the $\mathbf{q}=0$ selection rules of Table 1 to the present measurements, despite our sizeable \mathbf{q} . We will discuss the justification for this assumption in a moment.

In Figure 3 we show measurements with $\hat{\epsilon}_i || \hat{\mathbf{z}}$ and $\mathbf{q} || \hat{\mathbf{y}}$. In this geometry the Raman-active symmetries are $A_{1g} + E_{gx}$, and here the peak *vanishes*. The fluorescence yield (inset, taken *in-situ* with a second detector) shows a pronounced edge feature, the elastic scattering still appears in the spectra at the correct energies, and the selection rule-violating, incoherent continuum still appears in the energy-loss part of the spectrum. However the 5 eV peak is gone. We conclude that the 5 eV peak is symmetry-forbidden in this geometry, and by process of elimination that it has either B_{1g} or B_{2g} symmetry.

Armed with some knowledge of its energy and symmetry we are prepared to make a peak assignment. We appeal to the cell-perturbation calculations of *Simón et al.* [9], which is a treatment of the electronic structure of the undoped CuO_2 plane which emphasizes the symmetries of the states. We reproduce the central result in Figure 4. The ground state has pure b_{1g} symmetry, and starting at 4.3 eV above E_f there is an unbound band of a_{1g} symmetry. A transition from the ground state

to this band has the symmetry $b_{1g} \otimes a_{1g} = B_{1g}$, which with its energy is consistent with the experiment. There are no transitions of B_{2g} symmetry in the vicinity so we conclude that this is our peak.

We finish our discussion by describing how a nonzero \mathbf{q} should violate the selection rules of Table 1. For the simplistic case where ψ_{1s} and ψ_{4p} are tight-binding states the expression (5) generalizes to

$$[\Gamma(\psi_{4p}^* \psi_{4p} - \psi_{1s}^* \psi_{1s}) \otimes e^{i\mathbf{q}\cdot\mathbf{r}}] \otimes \Gamma(\psi_f^* \psi_i) \quad (6)$$

so the symmetries expressed in a given experimental geometry are those contained in the quantity $\Gamma(\psi_{4p}^* \psi_{4p} - \psi_{1s}^* \psi_{1s}) \otimes e^{i\mathbf{q}\cdot\mathbf{r}}$. Additional symmetries are made Raman-active by the symmetry-reducing effect of the exponential. For example, in the case $\hat{\epsilon}_i || \hat{\epsilon}_s || \hat{\mathbf{z}}$ in the optical limit the only Raman-active symmetry is A_{1g} . However with a nonzero $\mathbf{q} || \hat{\mathbf{x}}$ the symmetry is lowered to $A_{1g} + B_{1g} + E_{ux}$ [18]. So in general \mathbf{q} breaks the Raman selection rules - but not completely - and in principle can act as an additional probe of wave function symmetry.

A few words are in order about why we do not observe this expected breakdown of selection rules in our measurements, which should show up perhaps as a difference between Figs. 1 and 2 or more likely as a weak 5 eV intensity in Fig. 3. A fundamental shortcoming of group theory is that, while it will tell you if a given integral is nonzero, it tells you nothing about its *size*. RIXS data with improved statistics may yet observe such a breakdown.

Two improvements on our study would be, first, to employ a 90° scattering geometry as in the case of Refs. [7,8] to distinguish between the scattered polarization states. This would allow for complete, model-independent determination of the symmetry of the excitation (provided the effects of \mathbf{q} , which becomes sizeable at high scattering angles, remain unimportant). A second improvement would be to employ *space* group representation theory, since SCOC contains glide planes whose symmetry is not accounted for in a simple point group treatment.

We thank A. Bock, M. Rübhausen, and D. van der Marel for useful discussions, and especially G. A. Sawatzky for many heated debates. This work was supported by the NSF under grant DMR-9705131 and by the DOE under contract no. W-31-109-ENG-38.

- [4] O. Karis, A. Nilsson, M. Weinelt, T. Wiell, C. Puglia, N. Wassdahl, and N. Mårtensson, M Samant, and J. Stöhr, Phys. Rev. Lett. **76**, 1380 (1996)
- [5] P. M. Platzman and E. D. Isaacs, Phys Rev. B **57**, p. 11107 (1998)
- [6] P. Abbamonte, C. A. Burns, E. D. Isaacs, P. M. Platzman, L. L. Miller, S. W. Cheong, and M. V. Klein, Phys. Rev. Lett. **83**, 860 (1999)
- [7] Laurent C. Duda, Günter Dräger, Satoshi Tanaka, Akio Kotani, Jinghua Guo, Dirk Heumann, Sergej Bocharov, Nial Wassdahl, and Joseph Nordgren, Jap. J. Appl. Phys. **67**, 416 (1998)
- [8] Peter Kuiper, J.-H. Guo, Conny Sâthe, L.-C. Duda, and Joseph Nordgren, Phys. Rev. Lett. **80**, 5204 (1998)
- [9] M. E. Sîmon, A. A. Aligia, C. D. Batista, E. R. Gagliano, and F. Lema, Phys Rev. B **54**, R3780 (1996)
- [10] J. P. Hill, C.-C. Kao, W. A. L. Caliebe, M. Matsubara, A. Kotani, J. L. Peng, and R. L. Greene, Phys. Rev. Lett. **80**, 4967 (1998)
- [11] L. L. Miller, X. L. Wang, C. Stassis, D. C. Johnston, J. Faber, Jr., and C.-K. Loong, Phys. Rev. B, **41**, 1921 (1990)
- [12] T. Privalov, *et. al.*, Phys. Rev. B **59** 9243 (1999)
- [13] P. Skytt, P. Glans, J.-H. Guo, K. Gunnelin, C. Sâthe, J. Nordgren, F. Gel'mukhanov, A. Cesar, and H. Ågren, Phys. Rev. Lett. **77**, 5035 (1996)
- [14] A. Cesar, F. Gel'mukhanov, Y. Luo, H. Ågren, P. Skytt, P. Glans, J. Guo, K. Gunnelin, and J. Nordgren, J. Chem. Phys. **106**, 3439 (1997)
- [15] A relevant discussion of the continuum in inelastic scattering is in N. Ashcroft and D. Mermin, *Solid State Physics*, (Harcourt Brace College Publishers, Fort Worth, 1976), p. 474
- [16] P. M. Abbamonte, Ph.D. Dissertation, University of Illinois at Urbana-Champaign, January 1999
- [17] M. Tinkham, *Group Theory and Quantum Mechanics*, (McGraw-Hill, New York, 1964)
- [18] This can be verified with the spherical harmonic decomposition of Paolo Carra, Michele Fabrizio, and B. T. Thole, Phys. Rev. Lett. **74**, 3700 (1995)

TABLE I. Raman active symmetries for “indirect” transitions in all independent experimental geometries in the optical limit, $\mathbf{q}=0$. Symmetries are given both in the Schönflies and spherical harmonic notation.

Polarization (incident/scattered)	Raman Active Symmetries	
	Schönflies	Y_{lm}
$\hat{\mathbf{x}}/\hat{\mathbf{x}}$ or $\hat{\mathbf{y}}/\hat{\mathbf{y}}$	$A_{1g} + B_{1g}$	$s + d_{x^2 - y^2}$
$\hat{\mathbf{z}}/\hat{\mathbf{z}}$	A_{1g}	s
$\hat{\mathbf{x}}/\hat{\mathbf{y}}$ or $\hat{\mathbf{y}}/\hat{\mathbf{x}}$	$A_{1g} + B_{2g}$	$s + d_{xy}$
$\hat{\mathbf{x}}/\hat{\mathbf{z}}$ or $\hat{\mathbf{z}}/\hat{\mathbf{x}}$	$A_{1g} + E_{gx}$	$s + d_{xz}$
$\hat{\mathbf{y}}/\hat{\mathbf{z}}$ or $\hat{\mathbf{z}}/\hat{\mathbf{y}}$	$A_{1g} + E_{gy}$	$s + d_{yz}$

- [1] Michel van Veenendaal and Paolo Carra, Phys. Rev. Lett., **78**, 2839 (1997)
- [2] Faris Gel'mukhanov and Hans Ågren, Phys. Rev. B **57**, 2780 (1998)
- [3] See for example A. Moewes, S. Stadler, R. P. Winarski, D. L. Ederer, M. M. Grush, and T. A. Callcott, Phys. Rev. B, **58**, R15951 (1999)

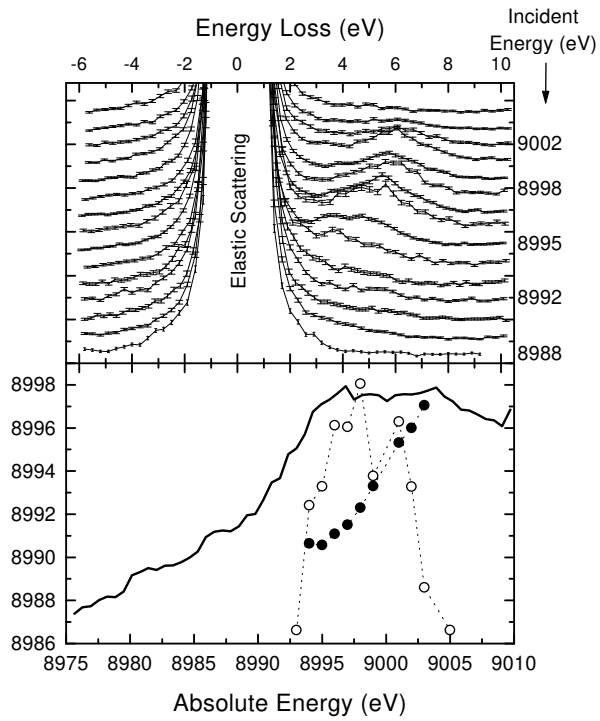


FIG. 1. RIXS spectra from SCOC for different incident energies, ω_i , with $\hat{\epsilon}_i \parallel (100)$ and $\mathbf{q} \parallel (001)$. The upper panel shows the individual scans (offset for clarity). In the lower panel the dark line is the fluorescence yield, showing the location of the edge. The open and filled circles are the inelastic peak height and its energy in absolute units, respectively, plotted against ω_i . In the $\mathbf{q}=0$ limit the Raman-active symmetries in this geometry are $A_{1g} + B_{1g} + B_{2g} + E_{gx}$.

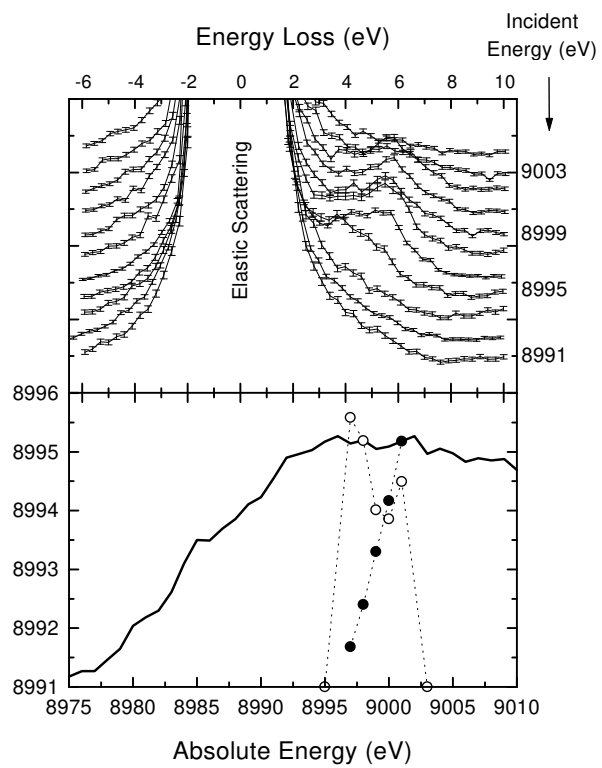


FIG. 2. The same measurement as shown in Fig. 1, however with \mathbf{q} now directed along $\hat{\mathbf{x}}$. In the optical limit this geometry contains the same symmetries as Fig. 1.

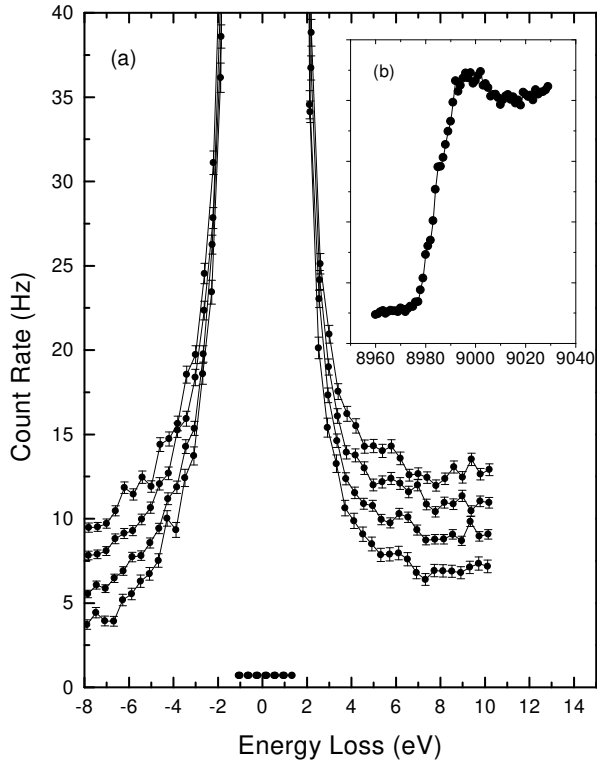


FIG. 3. The same measurements as in Figs. 1 and 2, however with $\hat{\epsilon}_i \parallel \hat{z}$. The fluorescence yield spectrum taken *in situ* is inset. The Raman-active symmetries in this geometry are $A_{1g} + E_{gx}$. The 5 eV peak, which likely has B_{1g} symmetry, is Raman-forbidden.

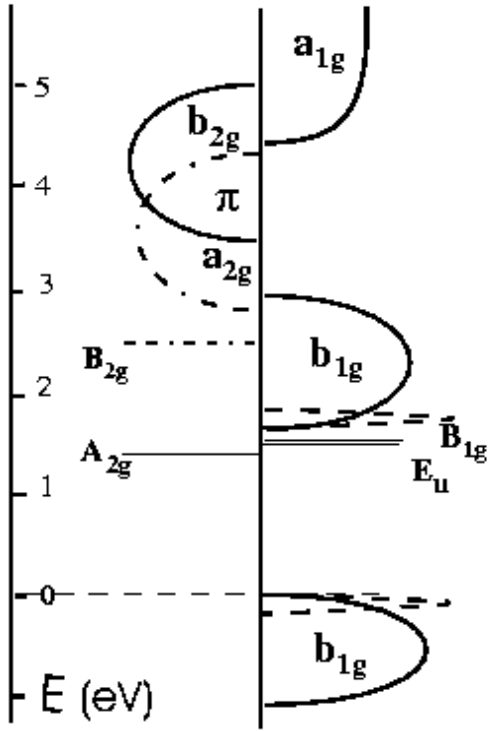


FIG. 4. Results of a cell-perturbation calculation, reproduced from Ref. [9]. The solid lines on the right hand side represent the dispersion of a native hole in the insulating CuO_2 plane. We assign our 5 eV feature to a transition from the b_{1g} ground state to the highest energy a_{1g} excited state.